

Integral field spectroscopy in the near infrared of NGC 3125-A and SBS 0335-052[★]

L. Vanzì¹, G. Cresci², M. Sauvage³, and R. Thompson⁴

¹ Department of Electrical Engineering and Center of Astro Engineering, Pontificia Universidad Católica de Chile, Av. Vicuña Mackenna 4860, Santiago, Chile
e-mail: lvanzi@ing.puc.cl

² INAF – Osservatorio Astrofisico di Arcetri, Largo E. Fermi 5, 50125 Firenze, Italy

³ Laboratoire AIM, CEA, Université Paris Diderot, IRFU/Service d'Astrophysique, Bât. 709, 91191 Gif-sur-Yvette, France

⁴ Steward Observatory, University of Arizona, Tucson, AZ 85721, USA

Received 2 June 2011 / Accepted 26 July 2011

ABSTRACT

We present integral field spectroscopy in the near infrared of the nearby dwarf starburst galaxy NGC 3125-A and of the low metallicity dwarf galaxy SBS 0335-052. The use of adaptive optics in the observations produces sub-arcsecond angular resolution. We pinpoint the star forming cores of both galaxies, identify relevant ISM components such as dust, photo ionized gas, shock excited gas and molecular gas. We relate these components to the large scale star formation process of the galaxies. In particular we find the emission of the near infrared lines of H₂ and especially [FeII] does not coincide with the HII region in NGC 3125. We have the first clear detection of [FeII] in SBS 0335-052.

Key words. galaxies: dwarf – galaxies: individual: NGC 3125 – galaxies: individual: SBS 0335-052 – galaxies: starburst

1. Introduction

In order to understand the processes that affect star formation on galactic scales, galaxy assembly, and evolution, we began a survey campaign to observe a number of nearby dwarf galaxies using near infrared integral field spectroscopy. In this way we have access to a number of unique features that characterize the star formation environment. As part of this investigation we have already published results on three relevant objects: II Zw 40 (Vanzì et al. 2008), He 2-10 and NGC 5253 (Cresci et al. 2010). All these galaxies are nearby irregular blue dwarfs undergoing powerful episodes of star formation, as such they reveal the details star formation on a large scale.

Here we report new observations of two other examples of this class of object: NGC 3125 and SBS 0335-052. We used AO correction to reach sub-arcsec angular resolution in our observations and in order to pinpoint the star forming cores of the galaxies.

Star formation in NGC 3125 (also known as Tol 3) occurs in a number of compact regions of which the most prominent ones were first indicated as 2 and 3 by Kunth et al. (1988) later renamed A and B by Vacca & Conti (1992) and Stevens et al. (2002). Those regions are separated by about 10 arcsec in a direction defining a PA = 124°. Both regions are further separated into two clusters respectively in HST images (see Hadfield & Crowther 2006). Clusters A1 and A2 are separated by about 0.5 arcsec, with cluster A1 dominating the emission in the HST/FOC *F220W* filter; clusters B1 and B2 are separated by about 0.2 arcsec and have similar luminosities in the mentioned band. NGC 3125 has characteristics similar to the three galaxies previously observed by us: relatively low mass, high star

formation rate per unit mass, presence of young massive clusters, WR features and irregular morphology. NGC 3125, however, differs from them in the radio continuum. Stevens et al. (2002) observed NGC 3125 in the radio at 6 and 3 cm and resolved the two regions A and B. Both regions show a negative spectral index indicating the predominance of non thermal radiation at those wavelengths. II Zw 40, He 2-10, and NGC 5253 instead are characterized by mostly thermal (bremsstrahlung) radio spectra (Beck et al. 2002; Johnson & Kobulnicky 2003; Turner et al. 1998). Spectra of NGC 3125 in the near infrared were observed by Vanzì et al. (2002), they found bright emission lines of H, He, and H₂ in 3125-A, much fainter lines in 3125-B. The metallicity is slightly sub-solar, Engelbracht et al. (2008) report $12 + \text{Log}(\text{O}/\text{H}) = 8.34$, about a factor 3 lower than in the sun. At a distance of 11.5 Mpc, 1 arcsec is equivalent to 55.7 pc. Because of our limited field of view we concentrated our observations on region A.

SBS 0335-052 was subject of several studies and observations in the past. Its interest resides mostly in the low metal content of the interstellar gas that was measured by Melnick et al. (1992) and Izotov et al. (1997) and found to be about 1/40 of the solar value. Despite initial thoughts, the idea that this galaxy might be a primeval object has been doubted (Östlin & Kunth 2001) and further weakened by the finding of a population of evolved stars in I Zw 18 a galaxy closer to us but characterized by even lower metallicity (Östlin & Mouhcine 2005; Aloisi et al. 2007). The stellar population in SBS 0335-052 cannot be resolved due to its large distance.

HST observations by Thuan et al. (1997) indicated that in this object star formation is occurring in a number of super star clusters, spanning a range of ages, the area covered by these clusters is about 2'' in length. The distance to SBS-0335-052 of 54.3 Mpc (Thuan et al. 1997) is significantly larger than for

[★] Based on observations obtained at the ESO-VLT under program 381.B-0132.

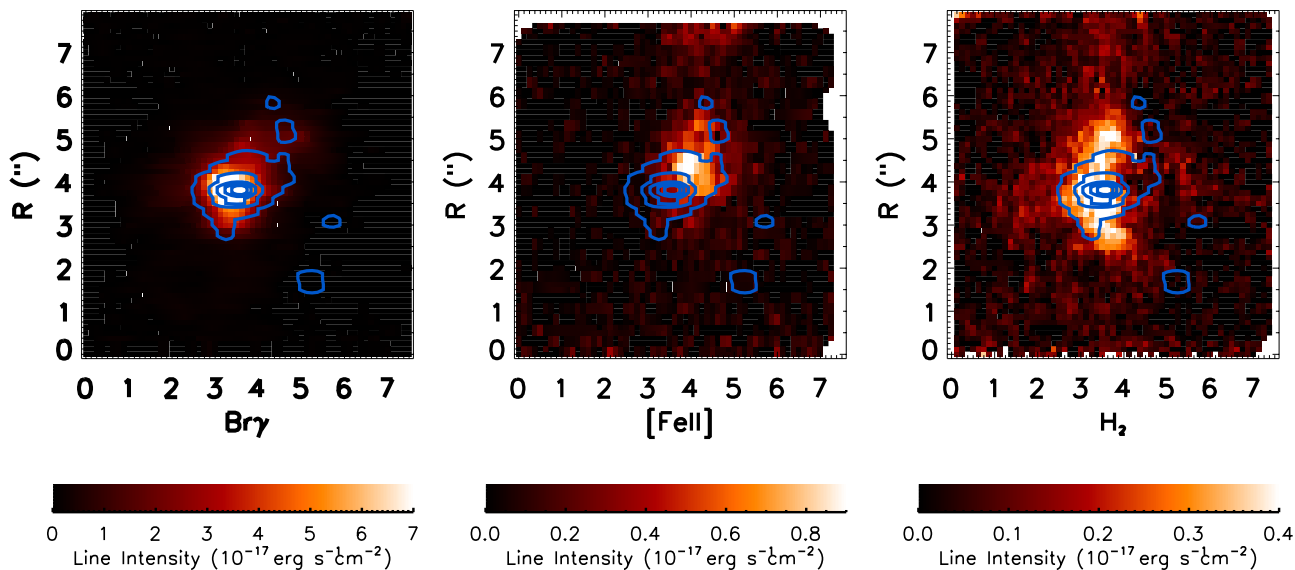


Fig. 1. Br γ , [FeII] and H $_2$ images of NGC 3125, the contours of the continuum are over plotted on each image. The continuum plotted corresponds to band H for [FeII] and to band K for Br γ and H $_2$.

NGC-3125, however the region of star forming activity in SBS-0335-052 has a linear size very similar to the distance between region A and B in NGC 3125, i.e. 526 pc. The galaxy was observed in the near infrared by Vanzi et al. (2000) and more recently by Thompson et al. (2006, 2009) with NICMOS on board HST. The optical clusters are also detected in the near IR and Thompson et al. (2009) find additional regions of very recent star formation not detected previously. Observations in the radio were obtained by Hunt et al. (2004) finding a composite thermal plus nonthermal slope.

This paper contains six main Sections, in Sect. 2 we present our new observations and data reduction, Sect. 3 is dedicated to the results on NGC 3125, Sect. 4 to the results on SBS 0335-052. Sections 3 and 4 are organized in five main parts: near IR continuum, ionized hydrogen, dust and extinction, molecular hydrogen, and ionized iron. In Sect. 5 we discuss the results of our work. Section 6 is the summary.

2. Observations

The observations were obtained with SINFONI at the ESO-VLT. SINFONI is a 3D near-IR spectrograph with AO correction (Eisenhauer et al. 2003).

For NGC 3125 we used the 0.250×0.125 arcsec/pixel scale which provides a field of view of 8 arcsec. For SBS 0335-052 we used the 0.100×0.050 arcsec/pixel with a field of view of 3 arcsec. The observations were performed with AO correction and laser guide star, this allowed to reach an angular resolution of approximately 0.25 arcsec, measured deconvolving the $FWHM$ of clusters with their angular size in HST images. We obtained spectra with the H and K grism, with an integration time of 20 min each and resolution of 2000 and 3000 respectively.

The data reduction was performed with the ESO pipeline and followed the standard steps of flatfielding, correction for dead/hot pixels, background subtraction and telluric correction. Flux calibration were carried out using A- and B-type stars, after removing the stellar features. Residuals from the OH line emission were minimized with the methods outlined in Davies (2007).

We compared both aperture photometry and emission line fluxes for the sources present in our fields that have previous observations in the literature and found good agreement in most cases (see Sects. 3.1 and 4.1), this makes us confident of the good level of reliability of our measures.

Integral field spectroscopy produces spectra for each pixel in our FOV thus providing spectral images at all observed wavelengths. Our analysis concentrated on a few features visible in the spectra, mainly the emission lines of atomic hydrogen, the emission lines of molecular hydrogen, the forbidden emission lines of ionized iron [FeII], and the nearby continuum. We extracted spectral images centered on these features. This was done by fitting a function to the continuum-subtracted spectral profile at each spatial position in the datacube. The function fitted was a convolution of a Gaussian with a spectrally unresolved emission line profile of a suitable sky line. The parameters of the Gaussian were adjusted until the convolved profile best matched the data, see Cresci et al. (2009) for further details.

3. Analysis of NGC 3125

In Fig. 1 we show the images in Br γ 2.167 μm , [FeII] 1.643 μm , and H $_2$ 2.121 μm rest wavelengths of NGC 3125-A with the contours of the continuum overplotted for reference. We will base our main analysis on these three images.

3.1. Near infrared continuum

The continuum emission of the field observed in NGC 3125 in the H and K band is dominated by one bright object corresponding to the center of the star forming region A. This source is significantly elongated in the EW direction and has a $FWHM$ of 2.5×4 pixels (0.3×0.5 arcsec). In addition to this bright source we detect a number of fainter nearby compact sources: in Fig. 2 we show the K continuum image with the sources detected identified by numbers according to decreasing K brightness. We extracted the photometry of source A from the spectra using the transmission curves of the H and K s filters and an aperture of radius 6 pixel, equivalent to 0.75 arcsec, and subtracted the background measured on a surrounding annulus.

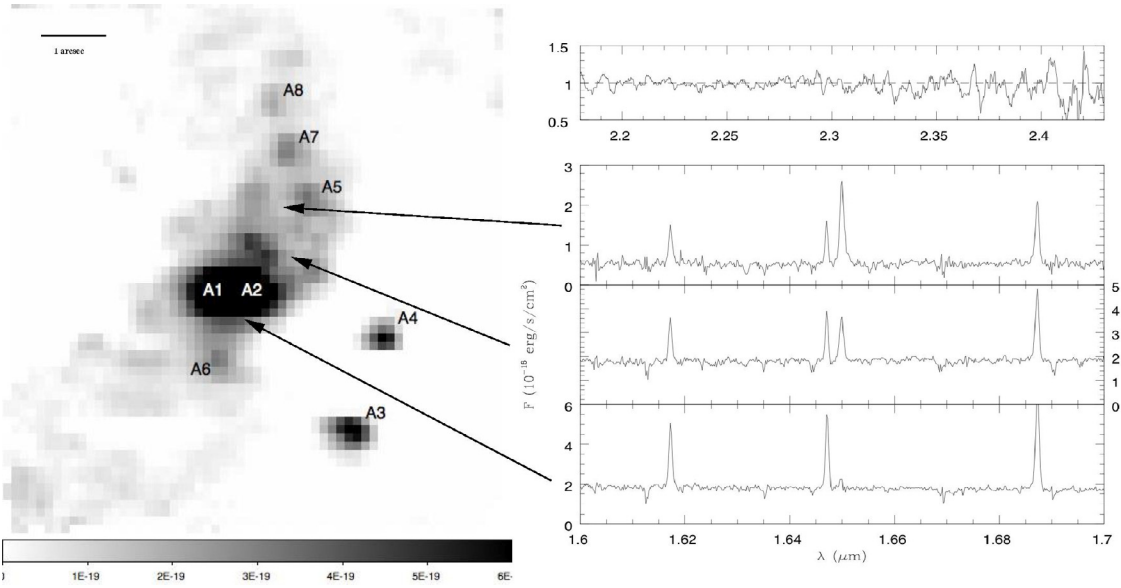


Fig. 2. In the *left panel* NGC 3125 in the K continuum, the compact sources detected are identified by numbers, the field of view is 8 arcsec, North is up, east to the left. In the *right panel* selected spectra extracted from the 3D data. At the top combined and normalized spectrum of the clusters 3, 4, and 8. The extraction regions of the other spectra are indicated by arrows.

The measured magnitudes are $H = 15.6$ and $K = 15.0$. For the same source Vanzì & Sauvage (2006) found $K = 14.81$, while Vanzì et al. (2002) $K = 14.97$, $H - K = 0.47$. The agreement is good considering that the previous observations were performed with a lower angular resolution. The fainter sources have K magnitudes around 18–19 and a color $H - K$ around 0.5–0.8. The aperture photometry of these sources is reported in Table 1. All sources observed appear resolved and have similar $FWHM$ of about 3 pixels or ~ 0.4 arcsec. Unfortunately we do not have a precise determination of the complex PSF produced by the AO system and we cannot deconvolve for it, therefore the values measured can only be considered upper limits, and they are equivalent to about 170 pc diameters. This size is on the upper side for super massive stellar clusters, so we can tentatively refer to these objects as super stellar clusters. The sizes measured in the HST images for A1 and A2 are much smaller, 0.17 and 0.13'' respectively. The larger sizes measured in the infrared may be due to an envelope of warm dust around the stellar cluster. Clusters A1/2, 5, 6 and 7 show a progression of ages from few to about 10 Myr as indicated by the equivalent width of Bry. We do not detect any emission lines in cluster 3, 4, and 8, so they are the oldest clusters observed in the field. They are also farther from source A than clusters 6 and 5.

We combined the spectra of these three clusters, in an attempt to increase the S/N, and have a weak detection of the stellar CO features beyond $2.29 \mu\text{m}$, compatible with the assumption that those are relatively evolved stellar clusters, older than 10 Myr. The spectrum is shown in Fig. 2.

3.2. Ionized hydrogen

The image obtained in Bry show the distribution of the ionized gas and identifies the main regions of star formation. We find that most star formation is concentrated in source A. The integrated Bry flux measured on this source with a radius of 0.5 arcsec is 4.5×10^{-15} erg/s/cm² with an eqw = 210 Å. Comparing the Bry equivalent width with the results of SB99 we derive an age younger than 4 Myr. We extracted from our data a spectrum centered on cluster A with the same aperture

Table 1. Aperture photometry and equivalent width of Bry for the clusters in NGC 3125.

Source	H	K	Bry eqw
A (1-2)	15.6	15.03	210
		14.81*	
		14.97**	
3	18.9	18.1	-
4	19.4	18.5	-
5	19.4	18.7	160
6	19.2	18.6	130
7	19.4	18.8	50
8	20.0	19.4	-

Notes. The aperture photometry was extracted with an aperture of 0.5 arcsec diameter, with the exception of cluster A (1-2) for which an aperture with diameter of 1.5 arcsec was used. (*) value from Vanzì & Sauvage (2006), (**) value from Vanzì et al. (2002). Equivalent width in Å.

as in Vanzì et al. (2002). We then compared our spectrum with theirs and found good agreement between the fluxes measured in the two observations.

We marginally resolve source A into two components that we identify with A1 and A2 according to the HST observations presented by Hadfield & Crowther (2006).

The bright Bry source is shifted by about 0.3 arcsec toward the east with respect to the peak of the brightest source of K continuum. This is easily explained with a picture of source A consisting of two clusters, A1 and A2 separated by 0.5 arcsec as given by HST images. While these sources are of comparable brightness in the K continuum, A1 dominates the line emission and it is much brighter in the UV (Hadfield & Crowther 2006). We therefore identify the peak of the Bry flux with A1. The peak of the K continuum falls approximately between A1 and A2.

A region of diffuse and much fainter Bry emission is detected around source A extending with plumes across our full field of view. Our observations, however, do not reveal the presence of other prominent compact sources.

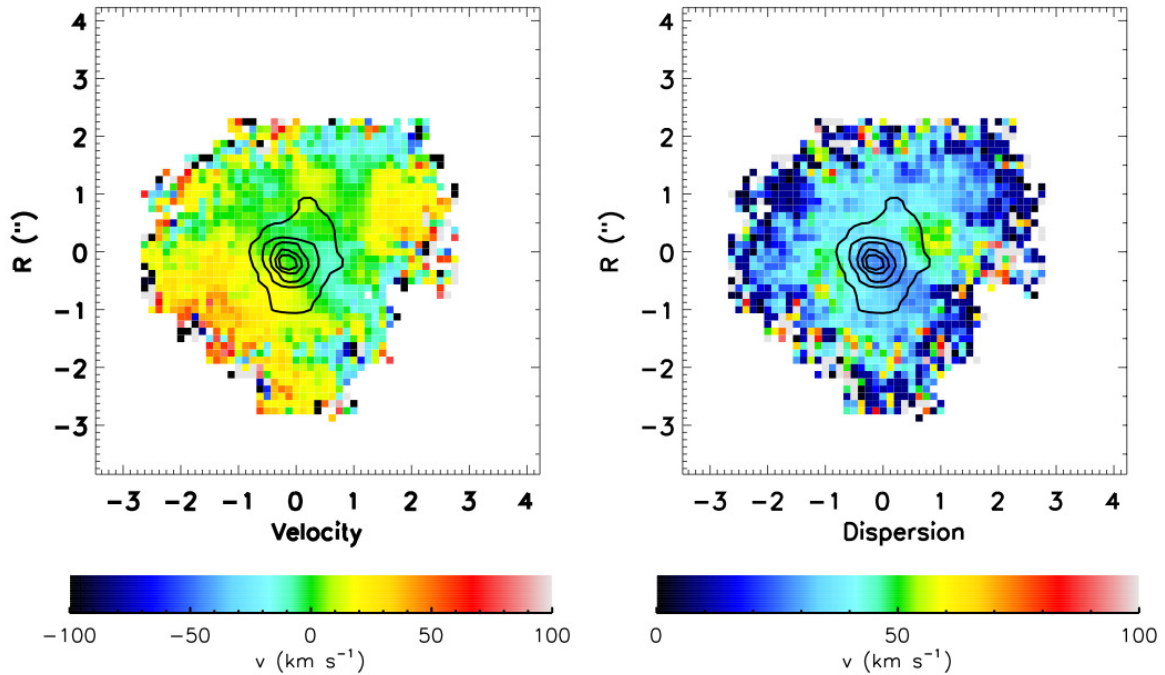


Fig. 3. Bry velocity field (*left panel*) and velocity dispersion (*right panel*) in NGC 3125. The contours represent the Bry emission.

The total Bry luminosity observed over our field of view, obtained by integrating on a circular aperture of radius 23 pix (2.87"), is 1.97×10^{38} erg/s. Correction for extinction (Sect. 3.3) produces a value of 3.47×10^{38} erg/s. This luminosity requires about 3300 equivalent O7V stars in terms of ionizing flux. Hadfield & Crowther (2006) estimate 2000 of such stars based on the $H\alpha$ flux. This difference indicates how in the near IR we observe deeper into the star forming region. We used SB99 (Leitherer et al. 1999) to calculate the total number of O stars required and obtained about 15 500.

Assuming a temperature of 10 000 K for the ionized gas and Case B recombination theory we derive a volume emission measure $(N_e)^2 V$ of $8.0 \times 10^{64} \text{ cm}^{-3}$ from the measured Bry emission. This is a factor of 270 less than the volume emission measure found by Thompson et al. (2009) for the sum of all of the sources in SBS0335-052E. This indicates that the star formation rate in SBS0335-052E is significantly greater than in NGC 3125.

In Fig. 3 (left panel) we present the velocity field derived from Bry, the Bry contours are overplotted on the image. The center of source A is set at 0 km s^{-1} and the velocity field is measured with respect to this reference. We observe possible evidence for a weak rotation around an axis crossing the galaxy in the NE to SW direction. Irregular patches with velocities up to +50 and down to -50 km s^{-1} are detected through the galaxy. These values are typical of the winds of ionized gas observed in blue dwarf galaxies (Martin 1999), though the interpretation of our observation in this sense is not straightforward based on the data available. The line width of Bry is typically of few tens km s^{-1} , see the velocity dispersion map on the right panel of Fig. 3. The spectral resolution is not high enough to detect any particular structure in velocity dispersion or in the line profiles that might provide a detailed study of the velocity structure, only a slightly higher dispersion is seen in an area to the NW of the center.

3.3. Dust and extinction

From the ratios of $H\alpha$, $H\beta$, and $H\gamma$, Hadfield & Crowther (2006) measured $E(B - V) = 0.24$ and 0.21 respectively on 3125-A and 3125-B, these values are equivalent to $A_V = 0.74$ and 0.65. Vacca & Conti (1992) measured $A_V = 1.24$ and 1.98 from $H\alpha$, $H\beta$. Galactic reddening is 0.25 mag. Vanzetti et al. (2002) measured the reddening from the ratio $\text{Pa}\beta/\text{Bry}$ and obtained $A_V = 1.6$ and 3.3 respectively on 3125-A and 3125-B.

Here we use the Bry and Br12 images to measure the extinction. We assumed an intrinsic ratio $\text{Br}12/\text{Bry} = 0.19$ corresponding to case B, $T_e = 10^4 \text{ K}$, and $n_e = 10^2 \text{ cm}^{-3}$ (Hummer & Storey 1987). We extracted spectra centered on A with a circular aperture of radius 8 pixel and measured $A_V = 4.8$ using the extinction law of Rieke & Lebofsky (1985) and $A_V = 5.4$ using the extinction law of Calzetti et al. (2000). We assumed the latter value considering the Calzetti's law more suitable for our case.

We obtained an extinction map but it does not show any particular structure except for a trend of higher extinction in correspondence of source A. The S/N is too low to determine any extinction structure beyond this.

We have already proved that our relative H to K calibration is reasonably good and in agreement with data from the literature, so we are confident that the results derived from the comparison of H and K spectra are reliable.

3.4. Molecular hydrogen

The image obtained in the line of H_2 (1-0)S(1) at $2.12 \mu\text{m}$, rest wavelength, gives a picture of the distribution of the molecular hydrogen in NGC 3125-A. This is very different from the morphology observed in Bry and in the continuum. The flux is relatively faint at the position of source A, while the diffuse emission extends further to the north and to the south. To facilitate

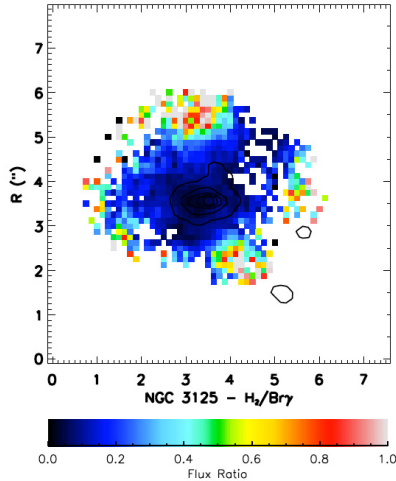


Fig. 4. Ratio of the line H_2 at $2.12 \mu\text{m}$ and $\text{Br}\gamma$ in NGC 3125.

Table 2. Molecular hydrogen lines detected in NGC 3125 and ratios to $(1-0)\text{S}(1)$.

Line	Line/(1-0)S(1)	Line	Line/(1-0)S(1)
(1-0)S(3)	0.30	(2-1)S(1)	0.5
(1-0)S(2)	0.25	(2-1)S(0)	0.5
(2-1)S(3)	0.32	(1-0)Q(1)	1.7
(2-1)S(2)	0.17	(1-0)Q(2)	0.45
(1-0)S(0)	0.45	(1-0)Q(3)	0.8

Notes. The errors on the ratios are smaller than about 20%.

the comparison in Fig. 4 we display the ratio $H_2/\text{Br}\gamma$. The ratio is lower toward the center of region A and higher further out indicating how the molecular hydrogen emitting region reaches beyond the ionized atomic hydrogen. We also see in Fig. 1 how the H_2 emission forms a bow like structure extended in the N-S direction and with its convexity toward the E.

A large number of hydrogen molecular lines are detected in addition to $(1-0)\text{S}(1)$. In Table 2 we report the measurements obtained from a spectrum centered on the region A. The comparison of the ratios with models (Black & van Dishoeck 1987) indicates fluorescence as the main mechanism of excitation. We took the line $(2, 1)\text{S}(1)$ as a reference because it is the brightest of those sensitive to the excitation mechanism and made a map of the ratio $(2-1)\text{S}(1)/(1-0)\text{S}(1)$. We found the ratio to be roughly constant at around 0.5 over the entire area observed, consistent with fluorescence. We infer therefore that UV photons from young massive stars are the main source of excitation of molecular hydrogen through out the area observed. The H_2 emitting region is shaped by the penetration of the UV photons and by the extent of the molecular cloud.

3.5. Ionized iron

More surprises are to be found when observing NGC 3125-A in the line of forbidden iron at $1.64 \mu\text{m}$. At this wavelength in fact the emission of the galaxy is shifted toward the north west by about 1 arcsec with respect to the underlying continuum. To make the difference more visible in Fig. 5 we show an image of the $[\text{FeII}]/\text{Br}\gamma$ ratio. The absolute value of the ratio is obtained re-scaling $[\text{FeII}]/\text{Br}12$ to $\text{Br}\gamma$, in this way we remove any systematic error produced by the H/K relative calibration and minimize the effect of extinction. The values span a range from about

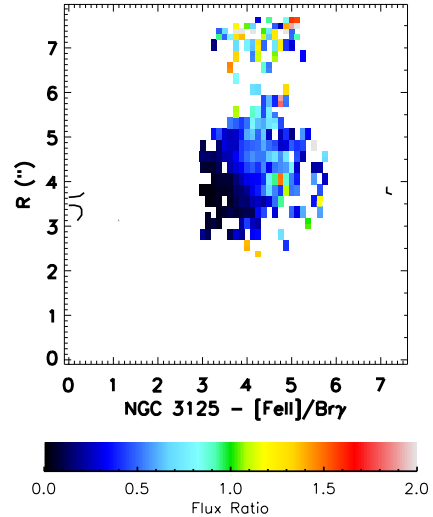


Fig. 5. Map of the $[\text{FeII}]/\text{Br}\gamma$ ratio for NGC 3125.

0.06, which is typical of photoionization, to values higher than 2 indicating significant contribution from SN remnants.

The area of bright $[\text{FeII}]$ emission is almost $2''$ long in the NS direction and more than $1''$ wide in the EW direction. It is close (0.4 arcsec) to the area of high velocity dispersion observed in $\text{Br}\gamma$ (see Fig. 3). According to Alonso-Herrero et al. (2003) it is possible to use the $[\text{FeII}]$ flux to estimate the number of SN remnants present in the observed field by comparing the $[\text{FeII}]$ luminosity with the estimated luminosity of a SN remnant. The $[\text{FeII}]$ flux observed is $9.14 \times 10^{-16} \text{ erg/s/cm}^2$, which gives a luminosity of $3.2 \times 10^{37} \text{ erg/s}$ corrected for extinction. From this value, using the calibration of $8 \times 10^{36} \text{ erg/s/SN}$ of Vanzani & Rieke (1997) we estimate about 4 SN remnants. Assuming a $[\text{FeII}]$ bright phase of about 10^4 yr we obtain a SN rate of $4 \times 10^{-4} \text{ yr}^{-1}$. The relation (1) of Cresci et al. (2010), which relates the $[\text{FeII}]$ luminosity with the SN rate through a constant $0.24 \times (10^{40} \text{ erg/syr})^{-1}$, gives instead $7 \times 10^{-4} \text{ yr}^{-1}$. These values can be compared with the SN rate derived by Stevens et al. (2002) for NGC 3125-A from radio observations of $4 \times 10^{-3} \text{ yr}^{-1}$, exactly 10 times higher. The sub-solar metallicity of the galaxy is not enough to explain the difference, as it is only a factor of about 3. Besides observational and calibration errors there is the possibility that even in the IR we do not see all the SNe detected in the radio. This may be due to extinction as proposed by Neff et al. (2004), Cresci et al. (2007), and Pérez-Torres et al. (2009).

It is interesting to compare the morphology of the $[\text{FeII}]$ with H_2 . In Fig. 6 we show the contours of the two lines. We observe that the $[\text{FeII}]$ emission almost fills the cavity left by the bow like structure of H_2 described previously. This observation will be discussed further in Sect. 5.

We detect two lines of $[\text{FeIII}]$ at 2.217 and $2.347 \mu\text{m}$ but at a much lower signal-to-noise, preventing us from obtaining reliable emission maps.

4. Analysis of SBS 0335-052

In Fig. 7 we show the images in $\text{Br}\gamma$ $2.167 \mu\text{m}$, $[\text{FeII}]$ $1.643 \mu\text{m}$, and H_2 $2.121 \mu\text{m}$ rest wavelengths of SBS 0335-05. The contours of the continuum are overplotted for reference. We will use these images as the base of our analysis as previously done.

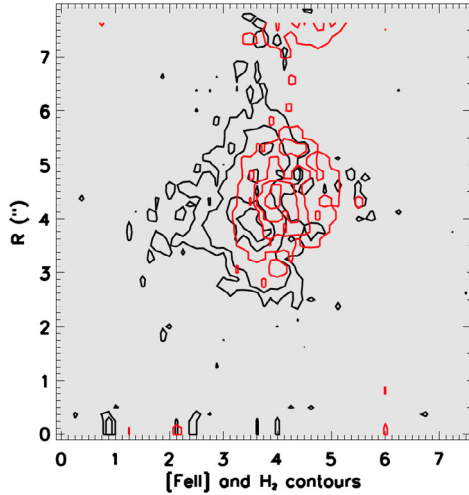


Fig. 6. Contours of H_2 (black lines) and [FeII] (red lines) in NGC 3125.

Table 3. Aperture photometry of clusters in SBS 0335-052.

Source	H (0.40)	H (0.88)	K (0.40)	K (0.88)
1–2	19.52	18.56	18.24 (18.45)	17.41 (17.55)
4–5	19.78	19.19	19.31 (19.32)	18.84 (18.37)

Notes. The apertures are indicated as diameters in arcsec. In parenthesis we report the values from Vanzi et al. (2000).

4.1. Near infrared continuum

A number of compact sources are detected in the H and K continuum mainly those named S1, S2, S3, and S4 by Thuan et al. (1997), see Fig. 8. We do not detect S7 (Thompson et al. 2009), while S6 (Thuan et al. 1997) and S8 (Thompson et al. 2009) fall out of our field of view. We compared the aperture photometry obtained on the sources detected in our observations with data from the literature similarly to Sect. 3.1 and found our observations fully consistent with previous ones. The results are reported in Table 3.

These sources span a sequence age of about 25 Myr according to Thuan et al. (1997) or 15–20 Myr according to Thompson et al. (2009) running from the north to the south with the oldest objects in the north near a SN bubble that supposedly triggered the star formation observed today. Since S4 is not detected in $Pa\alpha$ or Bry it is certainly older than 10 Myr and, in principle, should show features of a relatively evolved object. The H and K spectra of this object do not present any evidence of stellar absorption bands. In particular the CO bands at $2.29 \mu\text{m}$ are completely absent. We attribute this to the lack of metals in the galaxy. To quantify this better we use the results of SB99 (Leitherer et al. 1999) even though the model only reaches down to a metallicity of about 1/20 of solar. For this metallicity the CO index is basically 0 at an age of 10 Myr and less than a factor 2 below the solar value at an age of 30 Myr.

4.2. Ionized hydrogen

In Bry we detect the same sources detected by Thompson et al. (2009) in $Pa\alpha$ mainly S1, S2, S3- Pa shifted to the east of S3, and S7 to the west of S4 as it can be seen in the left panel of Fig. 7. To their analysis we can add the velocity field of the gas, showed in Fig. 9. The map is referred to 0 velocity on S1. Cluster S2 has a receding velocity of about $20\text{--}30 \text{ km s}^{-1}$, while S3 has a

similar velocity in the opposite direction. A part from this relative motion of the clusters no other velocity structure can be detected.

4.3. Dust and extinction

The presence of dust in SBS 0335-052 is certainly a complicated matter whose study gained relevance with the finding of Thuan et al. (1999) of an unexpected mid-IR excess attributed to thermal emission by dust and considered responsible for a A_V extinction of about 20 mag. The dust emission was later associated with source S1-S2 and the extinction measured directly $A_V = 12$ mag (Dale et al. 2001; Hunt et al. 2001). Hirashita et al. (2002) considered the presence of dust in low metallicity environment to be consistent with the amount of dust generated by type II SNe. The interpretation of the SED is far from being settled (Houck et al. 2004). Reines et al. (2008) and Johnson et al. (2009), based on the comparison of extinction and ionizing fluxes measured at different wavelengths, provide convincing evidence for a porous and clumpy ISM surrounding the natal clusters.

Previously Izotov et al. (1997) measured $A_V = 0.55$ from the Balmer decrement toward S1-S2. Vanzi et al. (2000) measured $A_V = 0.78$ from $H\beta/Bry$ and $A_V = 0.55$ from $H\alpha/H\beta$. Thompson et al. (2006) measured $A_V = 12$ from Bry and $Br\alpha$.

Our data are good enough to measure the extinction from the $Br12/Bry$ ratio towards S1, S2 and S3. For this purpose we extract spectra centered on each of these sources with radius of 3 pix. For all clusters we find consistently the same value: $A_V = 3.0$ mag. with the extinction law of Rieke & Lebowsky (1985) and $A_V = 3.4$ using the law of Calzetti et al. (2000).

We generated an extinction map over the entire Bry emitting region and found uniform extinction across it. This seems to indicate an extended absorbing cloud in which the star forming centers are embedded. We can then speculate that the clumpiness of the ISM must be on a scale smaller than our angular resolution.

For the extinction correction purpose we assume the picture of Reines et al. (2008) and correct for the value in magnitude measured at each wavelength +1 mag. for wavelengths shorter than $Br\alpha$, to take into account the 60% covering factor product of dense dust clumps.

4.4. Molecular hydrogen

Molecular hydrogen is detected in SBS 0335-052 only at the position of S1 and S2. Our new observations are mostly consistent with those of Vanzi et al. (2000) in all respects. The line ratios are all consistent with theirs and consistent with fluorescent excitation. Differently from them we do not detect the line $(2, 1)S(0)$. We compare carefully the spatial distribution of H_2 with Bry and [FeII] and differently from NGC 3125 we cannot detect any significant deviation. We measured the H_2 2.121 flux in S1 and S2 with the same apertures as Thompson et al. (2009) – $0.38''$ diameter – but obtained a total flux smaller by a factor 2. We attribute this difference to the combination of lower Strehl ratio provided by our AO observations, compared to HST, and the small apertures.

4.5. Ionized iron

We detect the [FeII] 1.64 forbidden emission line at both S1 and S2. Away from these two sources the flux drops and we do not

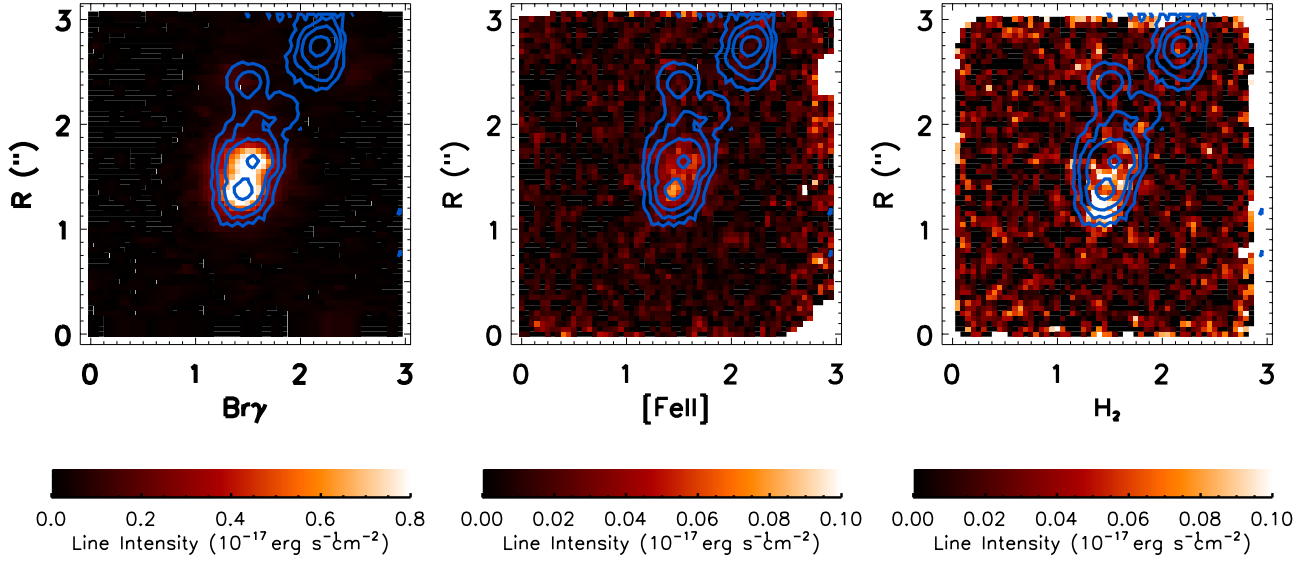


Fig. 7. Bry, [FeII] and H₂ images of SBS 0335-052, the contours of the continuum are over plotted on each image. The continuum plotted corresponds to band H for [FeII] and to band K for Bry and H₂.

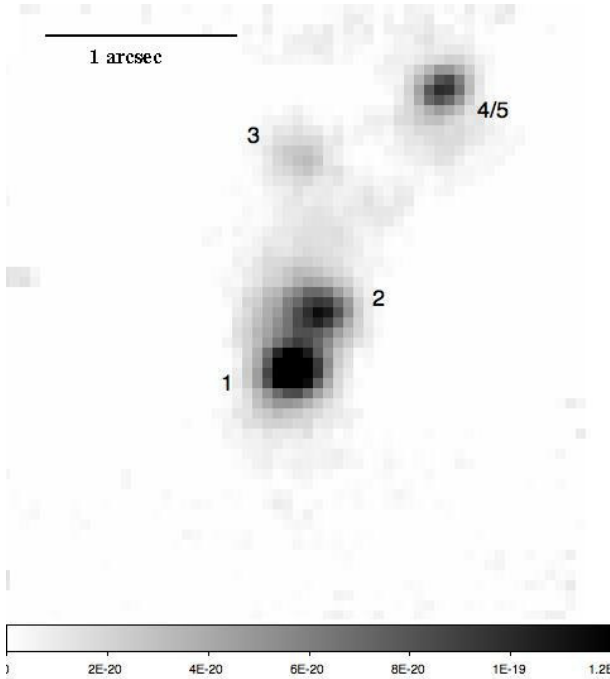


Fig. 8. SBS 0335-052 in the *K* continuum, the compact sources detected are identified by numbers, the field of view is 3.2 arcsec, North is up, east to the left.

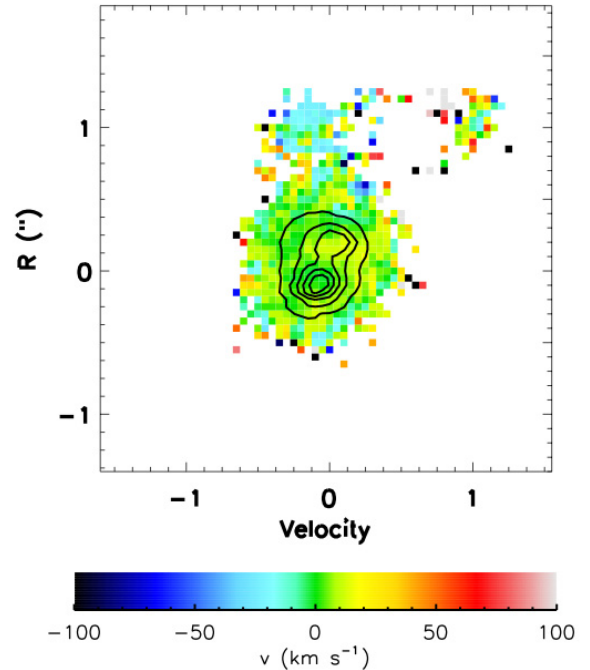


Fig. 9. Bry velocity field in SBS 0335-052 with Bry contours overplotted.

detect the line at S3 or at the position of any of the other clusters. The forbidden line of [FeII] 1.64 was not detected in SBS 0335-052 in earlier observations (Vanzi et al. 2000) and its absence interpreted to be consistent with the young age of the star forming episode. Our detection of the line, mostly due to the enhanced spectral resolution, allows some further consideration.

The ratio [FeII]/Bry on S1 and S2 is respectively 0.065 and 0.085 which was measured, as previously discussed, by rescaling from Br12. The error on the ratio is about 0.01. These values are consistent with photoionization by the clusters S1 and S2 at solar metallicity, however in our case they certainly exceed what should be expected because of the metal poor environment. For instance the models and measurements presented by

Lanfranchi & Matteucci (2010) would suggest that the iron has a relative abundance similar to oxygen. From the total flux observed by us in an aperture of 1.4'' in diameter, which includes both S1 and S2, of 7.4×10^{-17} erg/s/cm², we find a luminosity of 8.6×10^{37} erg/s, corrected for an extinction of $A_{1.64} = 0.36 + 1$ mag. To estimate the photoionized contribution to [FeII] we can multiply the Bry luminosity by a factor 0.06 which is the [FeII]/Bry photoionized ratio in a solar metallicity environment. The Bry observed flux of S1-S2 is 1.24×10^{-15} erg/s/cm² which is equivalent to a luminosity of 1.2×10^{39} erg/s when corrected for an extinction of $A_{2.16} = 0.18 + 1$ mag. It, therefore, gives a photoionized [FeII] luminosity of 7.2×10^{37} erg/s which still must be scaled down to the low metal abundance of the

galaxy. For this purpose we assume that iron scales as oxygen (Lanfranchi & Matteucci 2010) and apply a factor 1/40, giving 1.8×10^{36} erg/s. If this is correct photoionization provides only a small fraction (2%) of the observed [FeII]. Hunt et al. (2004) detect a radio continuum with a non thermal component which they associate with the clusters S1–S2 and consider consistent with the previously determined SN rate of 6×10^{-3} SN/yr (Hunt et al. 2001). However Johnson et al. (2009) find only marginal evidence for the presence of a non-thermal radio component. We wish to establish whether our observation is consistent with the SN rate reported in the literature. To do so we refer to relation (1) of Cresci et al. (2010), which relates the [FeII] luminosity to the SN rate using, as they do, a constant $\alpha = 0.24 \times (10^{40} \text{ erg/s yr})^{-1}$.

The [FeII] luminosity of 8.6×10^{37} erg/s would provide a SN rate of 2×10^{-3} SN/yr. The metallicity issue is even more complex in this case as, beside the abundance of the ISM, there is the unknown effect of the SN ejecta. In any case the SN rate calculated must be considered a lower limit, possibly to be scaled up by a factor 40. If we do so we end with 0.08 SN/yr, a factor 13 higher than the prediction of Hunt et al. (2001). These considerations would point to a bulk of the [FeII] emitted by SN remnants, with a possible excess of [FeII] that could be explained through the poorly known effect of metallicity or with a possible contribution of shocks generated by high stellar winds (Thompson et al. 2006).

In this picture the complete lack of [FeII] at the position of clusters S3, S4 and S5 is surprising. We can try to estimate the expected [FeII] flux from these sources by re-scaling the measurements of S1-S2. According to the *K* continuum measurements obtained by us and by Thompson et al. (2009) we can estimate that S3, S4, and S5 are less massive than S1 and S2 by a factor 10 or less. It is almost certainly less if we consider that the S1–S2 continuum must receive a nebular contribution from the ionized gas, while S3, S4, and S5 do not. Based on the *K* continuum we can assume that the S4-S5 complex is about 3 times less massive than S1-S2. We can also make a conservative assumption that half of the [FeII] luminosity from S1-S2 is photoionized even though a fraction of less than few % is certainly more realistic. We are then left with 4.3×10^{37} erg/s divided by a factor 3 to take into account the mass difference. The SN remnants, by conservative rescaling of the S1-S2 observation, then place lower limit on the S4-S5 [FeII] emission of about 1.4×10^{37} erg/s.

Our line detection limit in a circular aperture of radius 3 pix is about 10^{-18} erg/s/cm², equivalent to a line luminosity of 3.3×10^{35} erg/s. This is about 40 times lower than the expected lower limit on the luminosity of S4-S5. Why don't we observe [FeII] in the evolved clusters? The low abundance cannot be advocated in this case because we started our reasoning from values observed in the very same galaxy. We have two possible explanations: i) our mass re-scaling factor for S4-S5 is largely overestimated ii) S4-S4 are older than 40 Myr, or both. Our non detection of [FeII] at the location of evolved clusters goes together with the weak evidence for non-thermal radio emission. The situation of S4-S5 seems similar to clusters 3, 4, and 8 in NGC 3125. Those clusters, however, are more than 3 mag fainter in *K* than source A.

5. Discussion

In NGC 3125 we detect different sources of near infrared radiation. The continuum is mostly concentrated in one bright source, surrounded by a number of significantly fainter objects. We may consider these as a population of clusters that are relatively

evolved. The brightest source is a large region of recent star formation where there is more than one cluster present, two of which that we associate with the HST clusters A1 and A2.

The ionized gas is concentrated in one single source, HST cluster A1, which can be considered the main ionizing source of the entire region. This must be a young and massive cluster.

The ionized iron peaks at a position different from clusters A1 and A2 located about 1 arcsec to the north-west with an observed flux that is consistent with 4 SN remnants. This area must be the location of a previous episode of star formation with an age of less than 40 Myr. It is likely that the older star formation triggered the most recent one. Successive episodes of star formation triggering one another have been hypothesized (Cresci et al. 2010). This idea finds further support in the comparison of the distribution of [FeII] relative to H₂. We believe that the molecular hydrogen is mostly photoexcited by the young clusters and its distribution delineates somehow the molecular cloud which is currently undergoing star formation. We also show how this cloud forms a bow like structure with a cavity and how the emission of [FeII] almost fills that cavity, Fig. 6. If the [FeII] traces the effect of SN remnants produced in previous star formation we have a direct evidence of ISM compression and SF triggering by SNe. The distance between the center of [FeII] emission and the current star formation is about 1'' or 55 pc, equivalent to a traveling time of about 1 Myr for a shock speed of 50 km s⁻¹. The time required to produce the first SN is approximately 6 Myr, giving in total a delay time of about 7 Myr.

We may tentatively identify in NGC 3125 three episodes of massive star formation closely separated in time: the youngest episode that produced sources A1/2, 5, 6 and 7, a previous episode at the location of the bright [FeII] source, and the older clusters A3, 4 and 8.

In SBS 0335-052 we identify the population of clusters detected by HST in the visible and near-IR. We detect molecular hydrogen that is mostly fluorescently excited. The picture provided is fully consistent with previous observations. The study of the dynamics provides the picture of a relatively quiet galaxy. We detect for the first time the [FeII] forbidden line and we have difficulties in interpreting it quantitatively mainly because of the relatively poorly known effects of the metal abundance and of the [FeII] luminosity of SN. Based on what we believe reasonable hypothesis we find lack of [FeII] at the location of the most evolved clusters, possibly indicating for them an age older than previously thought.

If we compare all galaxies observed so far mainly, II Zw 40 (Vanzi et al. 2008), NGC 5253, He 2-10 (Cresci et al. 2010), NGC 3125 and SBS 0335-052, we can highlight the following points:

- 1) in all galaxies we observe young massive clusters. A few of them are younger than 2–3 Myr and are surrounded by large HII regions. Several others show evidence of star formation in the past few tens Myr;
- 2) the youngest clusters are also surrounded by areas of warm H₂ emitting in the near IR. These areas are much more extended than the HII regions in some cases such as NGC 3125, II Zw 40 and NGC 5253. In one case (II Zw 40) we could associate the H₂ to the CO molecular cloud observed in the mm. The H₂ is predominantly fluorescently excited. The case of SBS 0335-052 is somehow different as, at the angular resolution reached so far, the H₂ seems exactly associated to the HII region;
- 3) the regions of [FeII] emission appear spatially associated with the HII regions when photoionized as in II Zw 40.

However, when we observe evidence for shock excited [FeII] this appears to be spatially far from the HII region as in He 2-10 and NGC 3125. This picture is also observed in NGC 1569 (Pasquali et al. 2011). In SBS 0335-052 the [FeII] is presumably shocked and at the same location of the HII regions, however our spatial resolution is significantly lower for this galaxy. We can use the shock excited [FeII] as tracer of recent star formation, because SN would be present up to about 40 Myr after the start of an instantaneous burst of star formation. We therefore conclude that the formation of massive clusters, once triggered, migrates as SN appear, propagating itself through the galaxy where fresh molecular gas is available.

6. Conclusions

We obtained integral field spectroscopy in the near infrared of two blue dwarf galaxies: NGC 3125 and SBS 0335-052. The study of the spectral features observed provided a detailed view of the environment where the star formation is occurring. We found that:

1. NGC 3125 hosts a number of massive clusters spanning a range of ages, a similar result was already known for SBS 0335-052.
2. The molecular hydrogen is mostly fluorescently excited in both galaxies, however while in NGC 3125 it extends beyond the giant HII region around the youngest clusters, in SBS 0335-052 it appears to be concentrated in the giant HII regions associated to young clusters. The difference however could be only apparent due to the larger distance SBS 0335-052.
3. We detect [FeII] emission in both galaxies. In both cases the [FeII] luminosity is roughly consistent with the evolutionary stage of the galaxies and the SN rate derived from radio observations, once the effect of abundance is taken into account. In NGC 3125 the [FeII] emitting region is significantly separated from the HII region and the molecular hydrogen emitting region while in SBS 0335-052 it mostly coincides with them. Again this coincidence could be only apparent and produced by the larger distance. In SBS 0335-052 we do not detect [FeII] from relatively evolved clusters where we would have expected it.
4. The dust distribution is mostly uniform in both galaxies with a slightly higher concentration at the positions of the youngest clusters.
5. When considering all galaxies observed by us and similar results available in the literature in all of them we find evidence for self propagating star formation whose time scale is

consistent with the delay required to form SN at each location and a shock propagation speed of few tens km s^{-1} .

Acknowledgements. This research has made use of the NASA/IPAC Extragalactic Database (NED) which is operated by the Jet Propulsion Laboratory, California Institute of Technology, under contract with the National Aeronautics and Space Administration. LV received support from CONICYT through project Fondecyt No. 1095187 and project Anillo ACT-86. GC acknowledges support by the ASI-INAF grant I/009/10/0.

References

- Aloisi, A., Clementini, G., Tosi, M., et al. 2007, *ApJ*, 667, L151
 Alonso-Herrero, A., Rieke, G. H., Rieke, M. J., & Kelly, D. M. 2003, *AJ*, 125, 1210
 Beck, S. C., Turner, J. L., Langland-Shula, L. E., et al. 2002, *AJ*, 124, 132
 Black, J. H., & van Dishoeck, E. F. 1987, *ApJ*, 322, 412
 Calzetti, D., Armus, L., Bohlin, R. C., et al. 2000, *ApJ*, 533, 682
 Cresci, G., Mannucci, F., Della Valle, M., & Maiolino, R. 2007, *A&A*, 462, 927
 Cresci, G., Hicks, E. K. S., Genzel, R., et al. 2009, *ApJ*, 697, 115
 Cresci, G., Vanzì, L., Sauvage, M., & Van der Werf, P. 2010, *A&A*, 520, A82
 Dale, D. A., Helou, G., & Neugebauer, G. 2001, *AJ*, 122, 1736
 Davies, R. I. 2007, *MNRAS*, 375, 1099
 Eisenhauer, F., Abuters, R., Bickert, K., et al. 2003, *Proc. SPIE*, 4841, 1584
 Engelbracht, C. W., Rieke, G. H., Gordon, K. D., et al. 2008, *ApJ*, 678, 804
 Hadfield, L. J., & Crowther, P. A. 2006, *MNRAS*, 368, 1822
 Hirashita, H., Hunt, L. K., & Ferrara, A. 2002, *MNRAS*, 330, L19
 Houck, J. R., Charmandaris, V., Brandl, B. R., et al. 2004, *ApJS*, 154, 211
 Hummer, D. G., & Storey, P. J. 1987, *MNRAS*, 224, 801
 Hunt, L. K., Vanzì, L., & Thuan, T. X. 2001, *A&A*, 377, 66
 Hunt, L. K., Dyer, K. K., Thuan, T. X., & Ulvestad, J. S. 2004, *ApJ*, 606, 853
 Izotov, Y. I., Lipovetsky, V. A., Chaffee, F. H., et al. 1997, *ApJ*, 476, 698
 Kunth, D., Maurogordato, S., & Vigroux, L. 1988, *A&A*, 204, 10
 Johnson, K. E., & Kobulnicky, H. A. 2003, *ApJ*, 597, 923
 Johnson, K. E., Hunt, L. K., & Reines, A. E. 2009, *AJ*, 137, 3788
 Lanfranchi, G. A., & Matteucci, F. 2010, *A&A*, 512, A85
 Leitherer, C., Schaerer, D., Goldader, J. D., et al. 1999, *ApJS*, 123, 3
 Martin, C. L. 1999, *ApJ*, 506, 222
 Melnick, J., Heydari-Malayeri, M., & Leisy, P. 1992, *A&A*, 253, 16
 Neff, S. G., Ulvestad, J. S., & Teng, S. H. 2004, *ApJ*, 611, 1186
 Östlin, G., & Kunth, D. 2001, *A&A*, 371, 429
 Östlin, G., & Mouchine, M. 2005, *A&A*, 433, 797
 Pasquali, A., Bik, A., Zibetti, S., et al. 2011, *AJ*, 141, 132
 Pérez-Torres, M. A., Romero-Cañizales, C., Alberdi, A., & Polatidis, A. 2009, *A&A*, 507, L17
 Reines, A. E., Johnson, K. E., & Hunt, L. K. 2008, *AJ*, 136, 1415
 Rieke, G. H., & Lebofsky, M. J. 1985, *ApJ*, 288, 618
 Stevens, I. R., Forbes, D. A., & Norris, R. P. 2002, *MNRAS*, 1079, 1084
 Thompson, R. I., Sauvage, M., Kennicutt, R. C., et al. 2006, *ApJ*, 638, 176
 Thompson, R. I., Sauvage, M., Kennicutt, R. C., et al. 2009, *ApJ*, 691, 1068
 Thuan, T. X., Izotov, Y. I., & Lipovetsky, V. A. 1997, *ApJ*, 477, 661
 Thuan, T. X., Sauvage, M., & Madden, S. 1999, *ApJ*, 516, 783
 Turner, J. L., Ho, P. T. P., & Beck, S. C. 1998, *AJ*, 116, 1212
 Vacca, W. D., & Conti, P. S. 1992, *ApJ*, 401, 543
 Vanzì, L., & Rieke, G. H. 1997, *ApJ*, 479, 694
 Vanzì, L., & Sauvage, M. 2006, *A&A*, 448, 471
 Vanzì, L., Hunt, L. K., Thuan, T. X., & Izotov, Y. I. 2000, *A&A*, 363, 493
 Vanzì, L., Hunt, L. K., & Thuan, T. X. 2002, *A&A*, 390, 481
 Vanzì, L., Cresci, G., Telles, E., & Melnick, J. 2008, *A&A*, 486, 393